Reduced-Order Analysis of Turbulent Jet Noise

Michael Schlegel[1], Bernd R. Noack[1], Elmar Gröschel[2], Wolfgang Schröder[2],
Pierre Comte[3] & Peter Jordan[3]

[1] *Berlin University of Technology, D-10623 Berlin, Germany, Email: schlegel@pi.tu-berlin.de*
[2] *RWTH Aachen University, D-52062 Aachen, Germany*
[3] *CNRS UMR 6609 / University of Poitiers, F-86000 Poitiers, France*

Introduction

Targeting noise reduction, the goal of our modelling efforts is to provide a mechanistic understanding of noise generation in turbulent, subsonic jets. Thus, we perform flow decompositions, representing several optimal principles. In particular, a noise optimized flow decomposition into "loud" and "quiet" modes is performed by an extension of the proper orthogonal decomposition (POD) termed the most observable decomposition (MOD).

Data base

The hydrodynamic near-field and the aeroacoustic far-field are provided by numerical simulations. An ensemble of 725 snaphots of the three-dimensional velocity field $\mathbf{u}$ of a Ma=0.9, Re=3600 turbulent jet is calculated by a large eddy simulation [1]. The aeroacoustic far-field p is represented by 76 pressure sensors, situated at a line parallel to the jet axis (see Fig. 1). The sensor signals are determined by a Ffowcs Williams-Hawkings solver. The

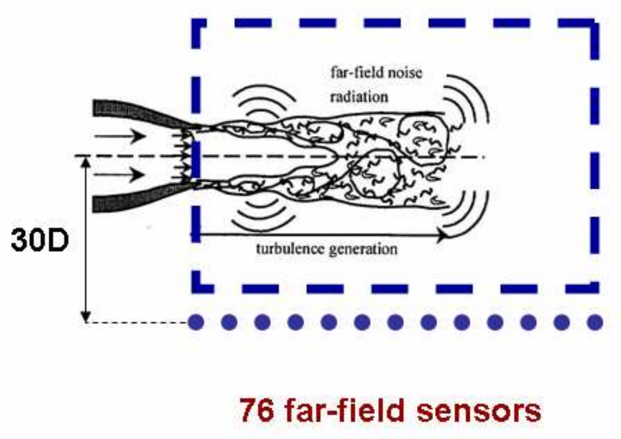

Fig. 1: Flow configuration.

Lamb vector field $\mathbf{L} = \mathbf{u} \times \nabla \times \mathbf{u}$ is considered as aeroacoustic source field, based on the Acoustic Pertubation Equation analogy proposed in [2]. A Reynolds decomposition has been carried out, which decomposes the velocity, aeroacoustic source and aeroacoustic far-field into the ensemble averages and fluctuating parts

$$\mathbf{u} = \langle \mathbf{u} \rangle + \mathbf{u}', \ \ \mathbf{L} = \langle \mathbf{L} \rangle + \mathbf{L}', \ \ p = \langle p \rangle + p', \qquad (1)$$

where the brackets $< \ldots >$ denote the time averaging operator $\langle \mathbf{u} \rangle = \lim\limits_{T\to\infty} \frac{1}{2T} \int\limits_{-T}^{T} dt\, \mathbf{u}$. The streamwise distributions of the fluctuation levels of $\mathbf{u}'$ and $\mathbf{L}'$,

$$K_{2D}(x) = \int dy\, dz \frac{\langle \mathbf{u}' \cdot \mathbf{u}' \rangle}{2}, \ \ Q_{2D}(x) = \int dy\, dz \frac{\langle \mathbf{L}' \cdot \mathbf{L}' \rangle}{2}, \quad (2)$$

are shown in Fig. 2. Both curves show a distinct peak level. The peak of the $Q_{2D}(x)$-curve is more pronounced and the curve drops off faster towards the end of the domain. This result indicates a bounded spatial extension of the acoustically active region, whereas the kinetic energy $K_{2D}(x)$ is still high in a downstream region.

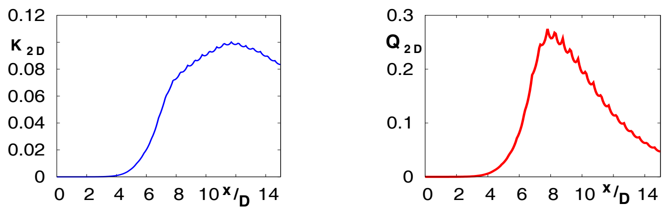

Fig. 2: Streamwise distribution of the fluctuation energy $K_{2D}(x)$ (left) and the fluctuation level of the aeroacoustic source $Q_{2D}(x)$ (right) over the streamwise component.

Azimuthal Fourier decomposition

An azimuthal Fourier decomposition is performed on the snapshot ensemble. In Fig. 3 the distribution of turbulent kinetic energy K_Ω (TKE) and aeroacoustic source level Q_Ω (ASL)

$$K_\Omega = \int\limits_\Omega d\mathbf{x}\, \frac{\langle \mathbf{u}' \cdot \mathbf{u}' \rangle}{2} \qquad Q_\Omega = \int\limits_\Omega d\mathbf{x}\, \frac{\langle \mathbf{L}' \cdot \mathbf{L}' \rangle}{2} \qquad (3)$$

is shown. More than 95% of TKE is contained in 21

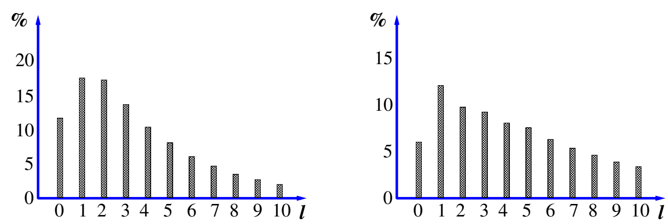

Fig. 3: Distribution of TKE (right) and ASL (left) in azimuthal Fourier subspaces. These distributions are displayed over the wavenumber l, where TKE of the azimuthal sine subspace and TKE of the azimuthal cosine subspace are summed up for each wavenumber.

azimuthal subspaces. The acoustically most important events are captured by these subspaces [3]. Moreover, more than 90% of ASL is contained in these 21 azimuthal subspaces.

Reduced-order representations

Reduced-order representations of velocity, aeroacoustic source and aeroacoustic far-field are performed utilising POD. Fluctuations are approximated by the linear expansion into POD modes

$$\mathbf{u}' \approx \sum_{i=1}^{K} a_i^{\mathbf{u}}(t)\,\mathbf{u_i}(\mathbf{x}), \quad \mathbf{L}' \approx \sum_{i=1}^{L} a_i^{\mathbf{L}}(t)\,\mathbf{L}_i(\mathbf{x}), \tag{4}$$

$$p' \approx \sum_{i=1}^{M} a_i^{p}(t)\,p_i(\mathbf{x}). \tag{5}$$

The POD modes $\mathbf{u_i}$ decompose the velocity most efficiently for TKE, whereas the POD modes $\mathbf{L_i}$ decompose the aeroacoustic source field most efficiently for ASL. The far-field POD modes p_i decompose the aeroacoustic source level most efficiently for the level of aeroacoustic far-field fluctuation, which is here termed noise

$$Z_\Gamma = \int_\Gamma d\mathbf{y}\, \frac{\langle p' \cdot p' \rangle}{2}. \tag{6}$$

POD is applied to each of the 21 azimuthal subspaces. Thus $725 \cdot 21 = 15225$ POD modes are determined. The residuals of the resulting reduced-order representation of velocity field and of aeroacoustic source field are shown in Fig. 4. Only 50% of TKE is resolved by the first 350

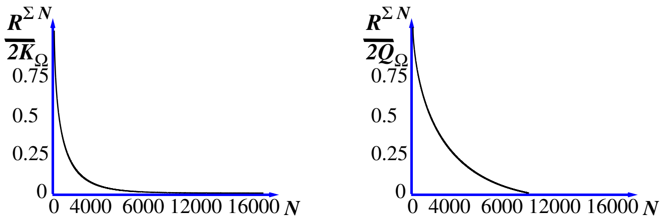

Fig. 4: Residuals of reduced order representations of velocity field (left) and of aeroacoustic source field (right). Unresolved TKE of the velocity field and unresolved ASL of the aeroacoustic source field are displayed relative to its total levels over the POD mode index.

POD modes $\mathbf{u_i}$ of velocity. Even more disenchanting for a straight forward reduced-order modelling, only 30% of ASL is resolved by the first 350 POD modes $\mathbf{L_i}$. Thus, a more goal-oriented reduced-order modelling strategy described in the next paragraph is motivated.

Further reduced-order representation results and details are contained in [1].

Loud and quiet flow modes

The POD of near-field velocity and far-field aeroacoustic field are utilised to construct loud and quiet flow modes $\mathbf{u_i^*}$, which decomposes the velocity fluctuation

$$\mathbf{u}' \approx \sum_{i=1}^{N} a_i^*(t)\,\mathbf{u_i^*}(\mathbf{x}) \tag{7}$$

most efficiently for correlated far-field noise

$$Z_\Gamma^C = \int_\Gamma d\mathbf{y}\, \frac{\langle p'(\mathbf{u}') \cdot p'(\mathbf{u}') \rangle}{2}, \tag{8}$$

introducing a relationship $p'(\mathbf{u}')$ of near- and far-field fluctuations. Thus, the construction of loud and quiet mode is attributed to the modelling of this relationship. In the MOD, a linear relationship

$$p' = \mathbf{C}\,\mathbf{u} \tag{9}$$

is proposed. $\mathbf{C}$ is produced by linear stochastic estimation, based on the Fourier coeffcients of near- and far-field POD, see [4]. The MOD modes are thus defined to be the pseudoinverse images of far-field POD modes

$$\mathbf{u_i^*} = \mathbf{C}^-\,p_i. \tag{10}$$

The MOD resolution of correlated noise is shown in Fig. 5. Surprisingly, more than 90% of the correlated noise is

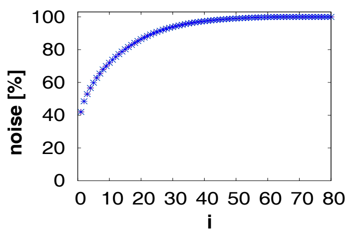

Fig. 5: MOD resolution. The cumulated resolution of correlated noise is displayed in percent over the MOD mode index.

resolved by only 24 MOD modes! Thus, the MOD method enables reduced-order modelling for the control of jet noise dynamics.

Further MOD results are detailed in [4].

References

[1] Gröschel, E., Schröder, W., Schlegel, M., Scouten, J., Noack, B.R. & Comte, P.: Reduced-order representation of turbulent jet flow and its noise source, CEMRACS 2005, published in: ESAIM Proceedings Vol. 16 (2007), 33-50

[2] Ewert, R. & Schröder, W.: Acoustic pertubation equations based on flow decomposition via source filtering, J. Comput. Physics 188 (2003), 365-398

[3] Michalke, A.: Some remarks on source coherence affecting jet noise, J. Sound Vibr. 87 (1983), 1-17

[4] Jordan, P., Tinney, C., Stalnov, O., Schlegel, M. & Noack, B.R.: Identifying noisy and quiet modes in a jet, AIAA-Paper in preparation